Journal of Power Sources 185 (2008) 512–518

Contents lists available at ScienceDirect

Journal of Power Sources

journal homepage: www.elsevier.com/locate/jpowsour

Fabrication and characterization of Fe_3O_4-based Cu nanostructured electrode for Li-ion battery☆

Huanan Duan[a], Joe Gnanaraj[b], Xiangping Chen[a,c], Boquan Li[a], Jianyu Liang[a,*]

[a] Department of Mechanical Engineering, Worcester Polytechnic Institute, Worcester, MA 01609, United States
[b] Yardney Technical Products, Inc., 82 Mechanic Street, Pawcatuck, CT 06379, United States
[c] College of Material Science & Technology, South China University of Technology, Guangzhou, Guangdong 510644, China

ARTICLE INFO

Article history:
Received 19 June 2008
Accepted 20 June 2008
Available online 9 July 2008

Keywords:
Nanostructured electrodes
Anode
Rapid rechargable Li-ion batteries
Template-assisted electrodeposition

ABSTRACT

Fe_3O_4-based Cu nanostructured electrodes for Li-ion cells are fabricated by a two-step electrochemical process. Cu nanorod arrays acting as current collectors are first prepared on a thin copper disk by alumina template-assisted electrodeposition. The active material of Fe_3O_4 is electrochemically deposited onto the Cu nanorod arrays by potentiostatic deposition. X-ray diffraction identifies textured growth for both the Cu nanorods and Fe_3O_4. Scanning electron microscopic observation further reveals that the active material are deposited between the Cu nanorods, and a 30 s deposition of Fe_3O_4 is sufficient to fill up the inter-rod space under the currently employed condition. Longer electroplating time leads to the coalescence of Fe_3O_4 particles and the formation of bulky Fe_3O_4 islands on the top of the Cu nanorods. Electrochemical properties of the nanostructured electrodes are studied by conventional charge/discharge tests. The results show that the rate capabilities of the nanostructured electrodes are better compared to those of the planar electrodes and the coalescence of Fe_3O_4 particles is detrimental to achieve sustained reversible capacities.

1. Introduction

Developing Li-ion batteries with high specific capacities and high current densities as power sources for many applications is of great interest [1–6]. It is now well accepted that the limitations in the rate capability of Li-ion batteries are mainly caused by slow solid-state diffusion of Li ions in the electrode materials [7,8]. Nanostructured materials are considered as active candidates to tackle the problem because of the potential advantages they offer, such as [9–11]: (i) short Li-ion transport length due to small particle sizes; (ii) fast surface reaction resulting from large electrode/electrolyte interface area; (iii) good accommodation of structure strains imposed by electrochemical reactions; and (iv) possibility of operation in systems with low electronic conductivity due to short path lengths for electron transport.

However, there are two major obstacles associated with nanostructured electrodes [10]. First, the increased electrode/electrolyte interface area leads to significant undesirable electrode/electrolyte side reactions, safety concerns and poor calendar life; second, the lack of control over the synthesis process and high expense to fabricate the electrode hinder the progress towards large scale production. To address the problem of side reactions with the electrolyte, a promising approach is to choose materials which fall within the stability window of the electrolyte or at least limit the formation of the solid-electrolyte interface layer, such as Fe_3O_4 (1.6 V versus Li^+(1 M)/Li) [12], $Li_{4+x}Ti_5O_{12}$ ($0 < x < 3$, 1.6 V versus Li^+(1 M)/Li) [10], and $Li_{0.91}TiO_2$–B (1.5–1.6 V versus Li^+(1 M)/Li) [13].

Fe_3O_4 is among a group of metal oxides that demonstrate a novel reactivity mechanism, the so called "conversion reaction", as summarized in Eq. (1)

$$M_xO_y + 2ye^- + 2yLi^+ \leftrightarrow xM^0 + yLi_2O \quad (1)$$

where M is a transition metal. This mechanism differs from the classical Li insertion/deinsertion process or Li-alloying reactions [1,12,18]. The use of Fe_3O_4 anode material reduces the overall cell voltage. But due to the high potential against lithium, side reactions with the electrolyte are minimized. Fe_3O_4 has a theoretical capacity around 928 mAh g^{-1} by assuming the reduction of Fe^{3+} and Fe^{2+} to Fe^0 during Li-ion intercalation, which is about three times that of commonly used graphitic carbons [12,21]. At room temperature the inverse spinel exhibits elec-

☆ Part of this work was presented at 10th Power Source R&D Symposium, Williamsburg, VA, August 20–23, 2007.

* Corresponding author. Tel.: +1 508 831 6649; fax: +1 508 831 5178.
E-mail address: jianyul@wpi.edu (J. Liang).

0378-7753/$ – see front matter © 2008 Elsevier B.V. All rights reserved.
doi:10.1016/j.jpowsour.2008.06.078

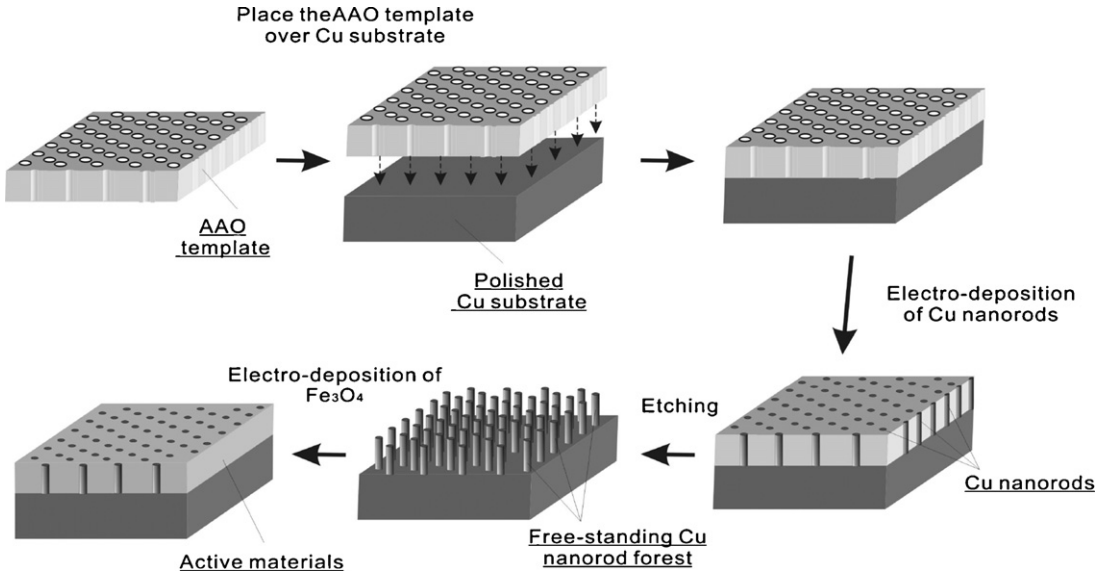

Fig. 1. Schematic of the fabrication of nanostructured electrodes.

tronic conductivity as high as 2×10^4 S m^{-1} [14]. So it is considered as a good candidate for nanostructured anode materials with enhanced safety, good capacity retention on cycling, and low self-discharge. In addition, magnetite is one of the cheapest common oxides and an environmentally friendly product with very low toxicity.

Efforts of studying iron oxides as Li intercalation material can be traced back to the 1980s, with more emphasis on lithiation of α-Fe_2O_3 (hematite) and spinel Fe_3O_4 in both non-aqueous electrolytes and molten salts [15,16]. However, slow kinetics of Li-ion intercalation/deintercalation among bulky iron oxides prevented further development. More recently, nanostructured hematite and magnetite attracted a lot of research interest as candidate electrode materials [1,9,12,17,18,21]. Usually, nanosized iron oxides were fabricated by various means, mixed with conducting acetylene black or Super P carbon, and pressed on current collectors such as Ni mesh or Li foil [12,17] to form working electrodes. Mitra et al. [18] employed polished planar Cu disks as the substrates for nanosized magnetite deposits through cathodic electrodeposition.

In this paper, we report our investigation of a new non-toxic nano-engineered electrode that is expected to shorten the Li-ion diffusion length. Our two-step electrode design consisted of the anodic aluminum oxide (AAO) template-assisted growth of Cu nanorods onto Cu disks as nanostructured current collectors and the electrochemical deposition of Fe_3O_4 onto the nano-architectured electrodes. Using such electrodes, we demonstrated improvement in rate capability compared to planar electrodes and good capacity retention at high rates over large number of cycles [19]. Our results suggests that the existence of nanorod current collectors provides better current collector/active materials surface contact and helpes maintain short diffusion length and accommodate structure strains imposed by electrode reactions.

2. Experimental

The fabrication process of Fe_3O_4-based Cu-nanostructured electrodes is schematically shown in Fig. 1. Key steps include (i) mechanical polishing of Cu substrates, (ii) fabrication of Cu nanorod arrays as current collectors, and (iii) electrochemical deposition of Fe_3O_4 onto the nanostructured current collectors. The key steps are described in more detail in the following sections.

2.1. Fabrication of Cu nanorod arrays as current collectors

Arrays of perpendicular Cu nanorods were fabricated by cathodic electrodeposition using a two-electrode configuration shown in Fig. 2. Two pieces of Cu disks (1.3 cm in diameter, from Yardney Technical Products, Inc.) served as the cathode and the anode. Before electrodeposition, the cathode Cu disk was mechanically polished with 1.0 μm alpha alumina and 0.05 μm gamma alumina polishing slurries (Buehler micropolish), followed by rinsing with deionized (DI) water and ultrasonically cleaning in ethanol. Oxide removal was carried out in a dilute HCl solution (1:9 in vol. ratio with water). The AAO template (Whatman, Anodisc 13, Cat. no. 6809-7023) was 60 μm thick, with a maximum porosity between 25% and 50%, pore size of 200 nm, and a pore density of 10^{10} cm^{-2} [20]. A cellulose paper separator (Whatman, Cat. no.: 1001042) was soaked with the electrolytic solution containing 100 g L^{-1} $CuSO_4 \cdot 5H_2O$ (Alfa Aesar), 20 g L^{-1} $(NH_4)_2SO_4$ (Alfa Aesar), and 80 mL L^{-1} diethylenetriamine (DETA, Alfa Aesar) [18]. The whole stack was kept under constant pressure by bolts and nuts. A Keithley Model 228A in a potentiostatic mode served as the power source.

The electrochemical depositions were carried out at 1.2 V DC at room temperature. After the electrodeposition, the cathodes were immersed in a 2 M NaOH solution for 15 min to remove the

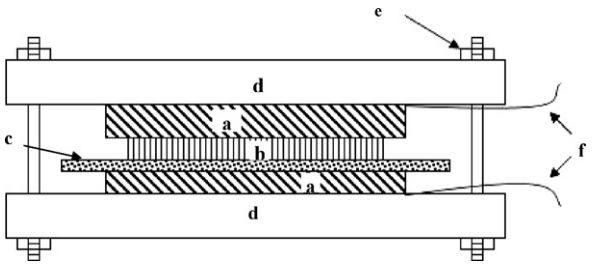

Fig. 2. Schematic of the cell for Cu nanorod electrodeposition: (a) copper plate, (b) alumina template, (c) cellulose membrane (separator), (d) plastic plate, (e) bolt and nut, (f) copper wire.

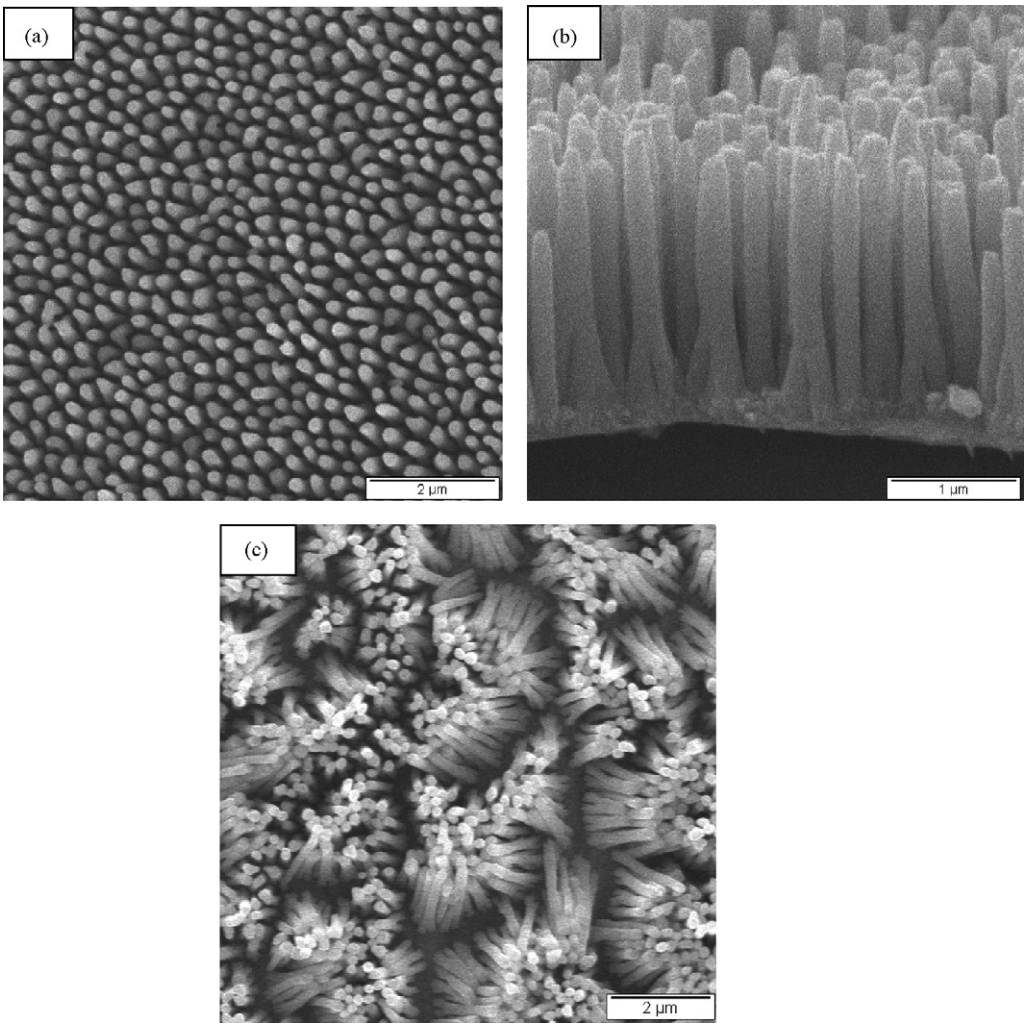

Fig. 3. SEM images of Cu nanorods grown on Cu substrate after removing the alumina template: (a) top view; (b) cross-section view of Cu nanorod arrays after 5 min deposition; (c) aggregated Cu nanorods after 10 min deposition.

AAO templates and cleaned in the dilute HCl solution to remove the surface oxides. The as-prepared samples are immediately used for Fe_3O_4 deposition to minimize the surface oxidation of the Cu nanorods.

2.2. Electrodeposition of Fe_3O_4

Fe_3O_4 was deposited on the Cu disks with Cu nanorod arrays by electrodeposition. The electrolyte consisted of 2 M NaOH (Alfa Aesar) and 0.09 M $Fe_2(SO_4)_3{\cdot}5H_2O$ (Alfa Aesar) complexed with 0.1 M tri-ethanol-amine (Acros Organics) at a pH value of 12.3 [18,21,22]. Electrodeposition was carried out in a two-electrode set-up at 1.5 V (DC) and 50 °C. The Cu disks with Cu nanorods served as the cathode and a graphite sheet served as the anode. After electrodeposition samples were rinsed with DI water and dried in air. Fe_3O_4 was also electrodeposited under the same conditions on mechanically polished planar Cu substrates to provide control samples.

2.3. Structure analysis and morphology characterization

The as-prepared nanostructured electrodes were examined by X-ray diffraction (XRD) using a REGAKU CN2182D5 diffractometer and scanning electron microscopy (SEM) using a JEOL JSM-840 microscope equipped with energy-dispersive X-ray spectroscopy (EDS).

2.4. Electrochemical tests

The electrochemical performance of our nanostructured electrodes was evaluated initially in coin cells. Coin/pouch half-cells were constructed using metallic lithium as the counter electrodes and the nanostructured electrodes as the anodes under argon atmosphere inside a glove box. The half-cells were cycled gal-

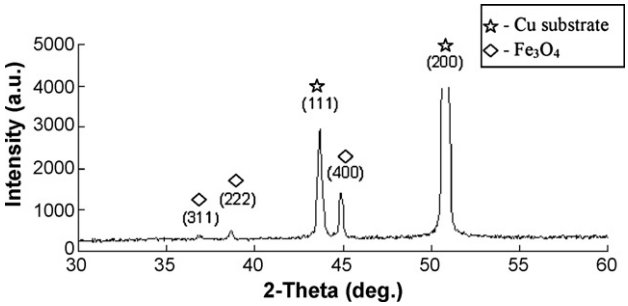

Fig. 4. XRD pattern of Fe_3O_4–Cu nanostructured electrode, star: metallic Cu, parallelogram: Fe_3O_4 deposit.

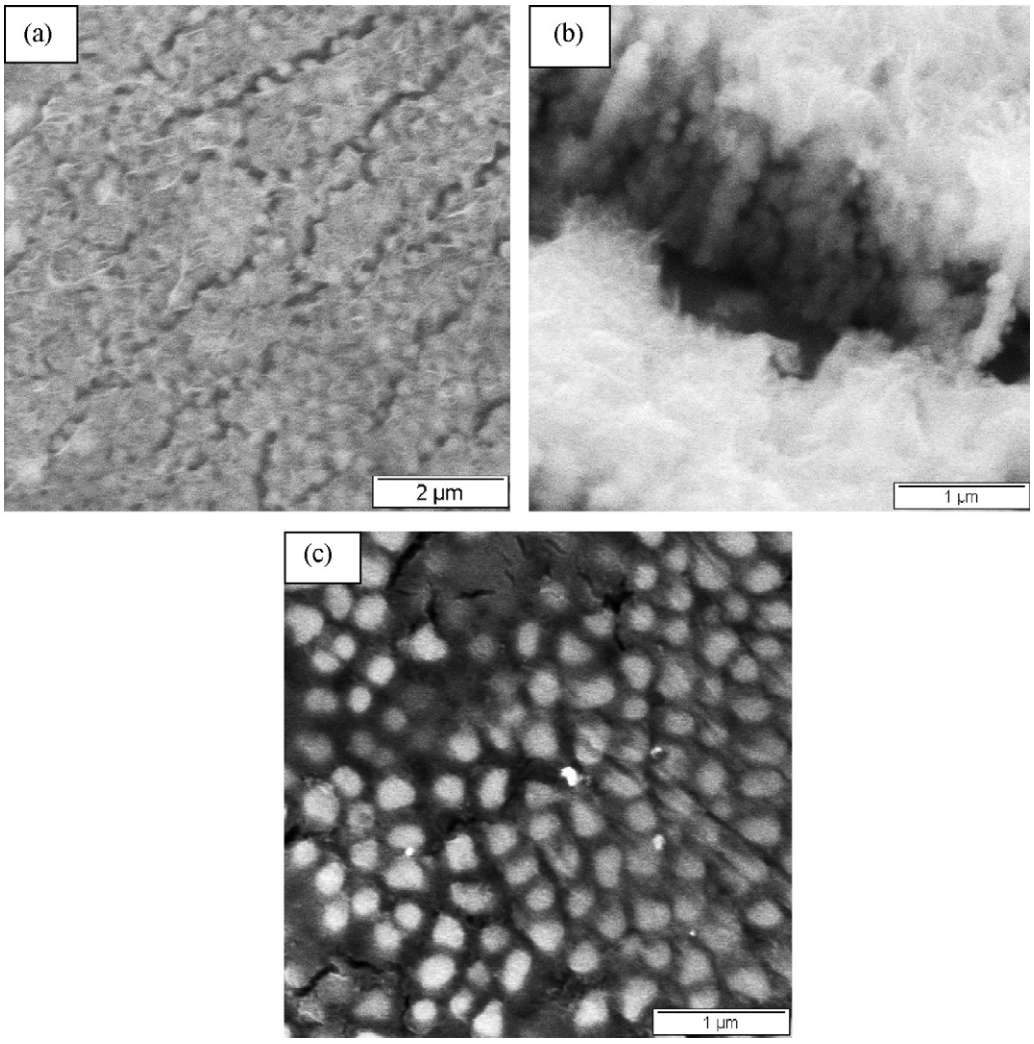

Fig. 5. SEM images of Fe_3O_4 deposit on Cu nanorods after 30 s electrodeposition: (a) top view, (b) oblique view, (c) same sample of (a) with top layer of Fe_3O_4 film removed.

vanostatically at a rate of *C*/20 and *C*/10, with *C* being defined as the full use of the capacity in 1 h. Full coin cells were fabricated using both the nanostructured electrodes and the control samples as the anodes and the standard $LiNi_{0.8}Co_{0.2}O_2$ (Yardney Lithion, Inc.) material as the cathodes. The cathodes were prepared by coating a paste containing 89% $LiNi_{0.8}Co_{0.2}O_2$, 2% Super P, 2% KS-15 graphite, 2% Shawinigan Acetylene Black (SAB), and 5% Kynar in *n*-methylpyrrolidone (NMP) onto Al foil. The loading of the

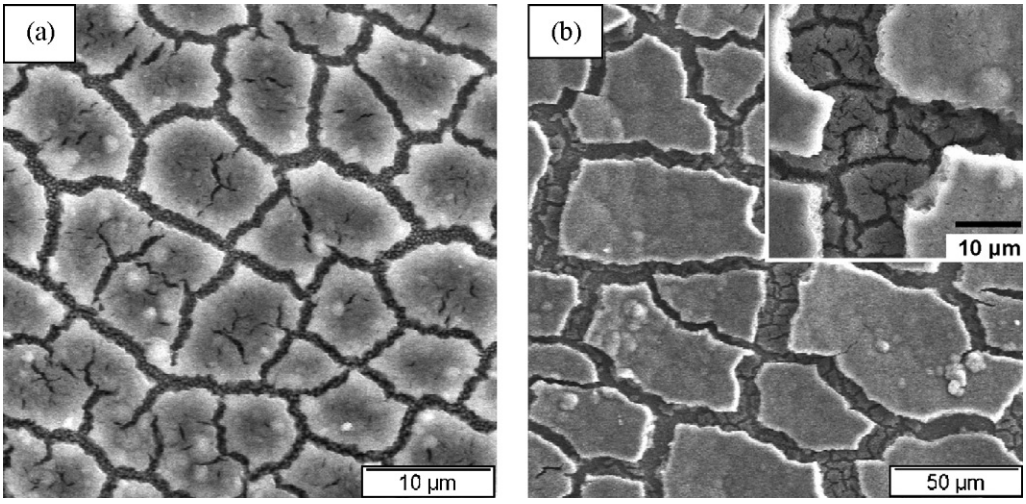

Fig. 6. SEM images of Fe_3O_4 nanostructured electrode after electrodeposition for (a) 60 s and (b) 300 s, inset: higher magnification image of (b).

cathode material was 0.0194 g cm^{-2}. Setela of 20 μm in thickness was used as the separators. The standard electrolyte of 1 M $LiPF_6$ (in ethylene carbonate (EC):dimethyl carbonate (DMC):diethyl carbonate (DEC)/1:1:1 in mass ratio) was used for both the half-cell and full-cell tests. The open circuit voltages of the fresh full-cells were about 220 mV. The coin cells were cycled under constant current conditions at different rates in the range of 1/10*C* to 10*C*. The charge/discharge capacities and the capacity retention property of the anodes at different charge/discharge current densities were studied.

3. Results and discussion

3.1. Nanostructured Cu current collector fabrication

Cu nanorods were electrodeposited on the surface of the mechanically polished Cu disks through the pores of an AAO template. This template-assisted deposition approach offers multiple advantages. For example, it is convenient to obtain uniform and free-standing Cu nanorod arrays. In addition, the deposition is cost-efficient, easy to control, and easy to scale up.

The uniformity in height of the deposited Cu nanorod arrays is expected to be of critical importance to the performance of the nanostructured electrode. It is significantly affected by the flatness of the Cu substrates. Atomic force microscope (AFM) study confirmed that mechanical polishing efficiently reduced the surface roughness of Cu foil. The measured area root mean square (RMS) roughness decreased from the original 83.0 nm to 16.3 nm after polishing, which helped to ensure an intimate contact between the cathode Cu disks and the AAO templates under mechanical pressure and to obtain an even current distribution on the electrodes during electrodeposition.

The use of the porous cellulose separator soaked with the electrolytic solution provided a media for Cu ions to transfer from the anode to the cathode uniformly, which helped the Cu nanorods grow at the similar speed. Since the use of porous cellulose separator eliminated electrolyte feeding, the process was greatly simplified and easy to control. The separator could also prevent short circuits, accommodate the mechanical constraints of the pressure applied to the stack, and eliminate undesirable electrolyte contamination.

Fig. 3 shows typical SEM images of the Cu nanorod arrays with the AAO template fully removed. Fig. 3(a) is the top view image of the Cu nanorods by 5 min electrodeposition. It shows that the polished Cu substrate surface has been covered by uniform and free-standing copper nanorods with an average diameter of 200 nm for each individual nanorod. As confirmed by our previous studies [23,24], the size of Cu nanorods is defined by the pore size of the AAO template. Fig. 3(b) is the SEM image of the cross-section. In Fig. 3(b), we can see that the nanorods are perpendicular to the substrate, their lengths are around 2 μm, and the inter-rod distance is less than 100 nm. The Cu nanorods tend to aggregate when the aspect ratio becomes large. For example, under the present deposition conditions, the nanorods began to aggregate when the deposition time was longer than 10 min as shown in Fig. 3(c). Aggregation is detrimental to the subsequent loading of Fe_3O_4 because Fe_3O_4 particles tend to crystallize over the top of the Cu nanorod bundles instead of on the surface of individual Cu nanorods and lose the advantages provided by the nanostructured current collectors.

3.2. Electrodeposition of Fe_3O_4

Fig. 4 is a typical XRD pattern from the as-prepared nanostructured electrodes. The two strong peaks at around 43.3° and 50.5°

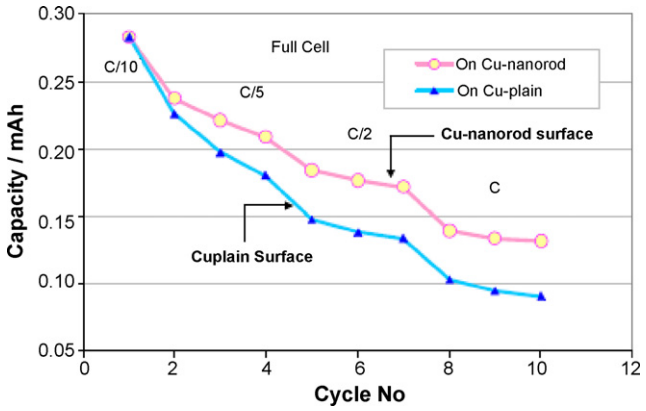

Fig. 7. Charge capacity versus cycle number of full coin cells cycled at different rates between C/10 and C. For both electrodes, the Fe_3O_4 electrodeposition time was 120 s. Note that the geometrical surface area of the copper disk was 1.26 cm^2.

correspond to the Cu(1 1 1) and the Cu(2 0 0) reflections (International Centre for Diffraction Data card no. 04-0836), originating from the Cu substrate and the Cu nanorods. The Cu(2 0 0) reflection is much stronger than that of Cu(1 1 1), suggesting that the Cu substrate and the Cu nanorods are [1 0 0] textured. The three weak reflections can be assigned to (3 1 1), (2 2 2), and (4 0 0) of magnetite Fe_3O_4 phase (ICDD no. 26-1136), with the (4 0 0) reflection the strongest. This indicates that the Fe_3O_4 nanoparticles are not randomly attached to the Cu nanorods, but showing preferred orientation.

Fig. 5 shows the SEM images of the nanostructured electrode after 30 s Fe_3O_4 deposition. Fig. 5(a) and (b) clearly show that Fe_3O_4 filled up the spaces between the Cu nanorods and began to coalesce into a continuous thin layer on the top of the Cu nanorod arrays with small cracks forming in some areas. The oblique view in Fig. 5(b) demonstrates that Fe_3O_4 was deposited on the surface of individual Cu nanorods. Clearly, Fe_3O_4 deposited between the Cu nanorods is well maintained to be nanostructured due to the small inter-rod spaces, which is crucial to gain the advantages of nanomaterials such as shortened Li-ion diffusion length. Fig. 5(c) shows the top view of the same sample after the top thin Fe_3O_4 layer was carefully removed by polishing. It confirms that the Fe_3O_4 has been deposited into the Cu nanorod array. The corresponding EDX spectrum (not shown) verifies the presence of the elements of Fe, O, and Cu in the area of Fig. 5(c).

When the deposition time was increased to 60 s, the Fe_3O_4 film became thick and bulky islands with average size around 10 μm with large cracks were evident as shown in Fig. 6(a). One possible reason for the crack generation is the different volume change of Fe_3O_4 deposit and Cu nanorod arrays during sample drying. Fig. 6(b) indicates that long deposition time of 300 s led to the formation of even thicker and bigger Fe_3O_4 islands with size up to tens of micrometers. The inset shows that the big islands formed right above the small islands in Fig. 6(a). These micron-sized Fe_3O_4 islands are undesirable for nanostructured electrodes because they may block the passage of electrolyte and Li-ion and prevent us from taking the advantages provided by Cu nanorod currently collectors.

3.3. Pouch/coin cell cycling tests

The full coin cells were cycled at various constant current rates. Fig. 7 compares the charge capacities of the coin cells with the nanostructured and the planar control electrodes at current rates between *C*/10 and *C*. For comparison, Fe_3O_4 electrodeposition conditions were kept the same and a 120 s deposition time was used for both samples. The cell with the nanostructured Fe_3O_4 electrodes

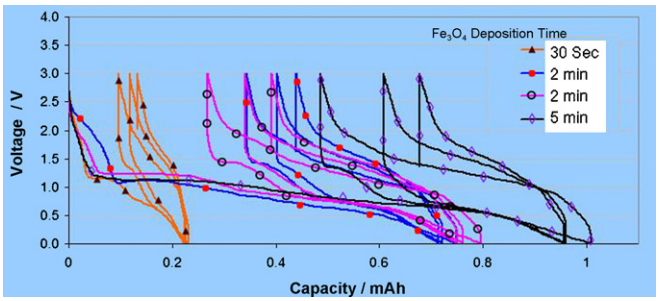

Fig. 8. Potential–capacity profiles of the as-prepared nanostructured electrodes with different Fe_3O_4 deposition time galvanostatically cycled versus Li at a rate of $C/20$ for the first cycle and $C/10$ for the second and the third. Note that the geometrical surface area of the copper disk was 1.26 cm^2.

demonstrated better rate capabilities at high current rates compared to the planar ones, though they exhibited similar capacities at low current rate of C/10. Fig. 7 stresses the benefit of having a nanostructured current collector compared to a planar one in terms of power density.

The half-cell test results of the nanostructured electrodes with Fe_3O_4 deposition durations of 30 s, 120 s and 300 s are presented in Fig. 8. It shows that all the nanostructured electrodes behaved alike during the first several cycles, demonstrating the characteristic electrochemical signature of the conversion reactions involved in transition metal oxide during charging and discharging [1,21]. The potential dropped rapidly to reach a well-defined plateau below 1 V corresponding to the full reduction of Fe_3O_4 into the Fe^0/Li_2O mixture [21]. On cycling, the common charge/discharge hysteretic profiles which are inherent to conversion reactions were maintained. The sample with 300 s Fe_3O_4 deposition time exhibited the largest capacity compared to the other three, which is expected since longer deposition promises more active materials. Fig. 8 also shows that the capacity retention of electrodes with longer deposition durations, i.e. 120 s and 300 s, deteriorated faster than those with shorter deposition time, i.e. 30 s, which is consistent with Tarascon's work [18,21]. The electrode Coulombic efficiency is higher for electrodes with a short Fe_3O_4 deposition time. A value of 88% was obtained after three cycles for a deposition time of 30 s compared to 80% for the 300 s deposition.

Fig. 9 shows the charge/discharge capacity profiles of the nanostructured electrodes with different Fe_3O_4 deposition time cycled at various current rates. It is notable that the capacity of the electrode with 30 s Fe_3O_4 deposit demonstrated the best sustained reversible capacity through out the whole cycling process, indicating the electrochemical and mechanical robustness of the electrode. SEM observation after cycling tests revealed no significant morphology change of either the Fe_3O_4 deposits or the Cu nanorods (inset in Fig. 9). In contrast, the capacities of the electrode with 5 min Fe_3O_4 deposition dropped fastest with increasing cycle numbers and those of the electrode with 2 min deposition dropped intermediately.

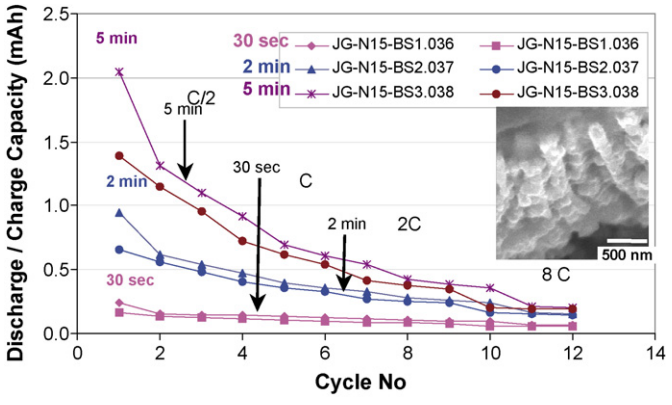

Fig. 9. The capacity retention of a Fe_3O_4 film electrodeposited onto nanostructured copper substrate for different time and cycled at a variety of rates. Inset: SEM image of the electrode with 30 s Fe_3O_4 deposition after cycling tests.

These half-cell test results, combined with the observation in Fig. 6, strongly suggest that as the time for Fe_3O_4 deposition elapses and the polycrystalline Fe_3O_4 particles aggregate into micron-sized islands above the Cu nanorod arrays, these islands tend to block the access of electrolyte to the inter-nanorod spaces, cause loss of the advantages of nanostructured material, and are undesirable for capacity retention during charge/discharge cycling.

4. Conclusions

The current work develops a nanostructured anode material for Li-ion battery by a two-step fabrication process. This process consists of the AAO template-assisted growth of Cu nanorods onto Cu substrates as nanostructured current collectors followed by the Fe_3O_4 electrodeposition. Uniform and free-standing Cu nanorod arrays were deposited onto mechanically polished Cu disks and the active material of Fe_3O_4 was successfully grown on the surface of individual Cu nanorods. The nanostructured electrode showed superior rate capabilities compared to the planar control samples. It was also observed that the formation of micron-sized Fe_3O_4 islands led to deteriorated reversible capacity retention.

Acknowledgements

The financial support for this work from NASA (contract no. NNJ07JB33C) & OSD/ONR (contract no. N00014-07-M-0110; 07PR06126-00) are gratefully acknowledged. We thank Prof. Robert Thompson for his help during this work. We also want to thank Prof. Nancy Burnham for her help in AFM analysis.

References

[1] P. Poizot, S. Laruelle, S. Grugeon, L. Dupont, J.M. Tarascon, Nature 407 (2000) 496–499.
[2] N. Li, C.R. Martin, B. Scrosati, J. Power Sources 97–98 (2001) 240–243.
[3] X. He, W. Pu, L. Wang, J. Ren, C. Jiang, C. Wan, Electrochim. Acta 11 (2007) 3651–3653.
[4] V. Subramanian, A. Karki, K.I. Gnanasekar, F. Eddy, B. Rambabu, J. Power Sources 159 (2006) 186–192.
[5] H. Wang, T. Abe, S. Maruyama, Y. Iriyama, Z. Ogumi, K. Yoshikawa, Adv. Mater. 17 (2005) 2857–2860.
[6] M. Park, Y. Kang, G. Wang, S. Dou, H. Liu, Adv. Funct. Mater. 18 (2008) 455–461.
[7] J. Li, Z. Tang, Z. Zhang, Electrochem. Commun. 7 (2005) 62–67.
[8] P.G. Bruce, Chem. Commun. 19 (1997) 1817–1824.
[9] E. Hosono, S. Fujihara, I. Honma, M. Ichihara, H. Zhou, J. Electrochem. Soc. 153 (2006), A1273–A1278.
[10] A.S. Arico, P. Bruce, B. Scrosati, J.M. Tarascon, W.V. Schalkwijk, Nature Mater. 4 (2005) 366–377.
[11] C.R. Sides, N. Li, C.J. Patrissi, B. Scrosati, C.R. Martin, MRS Bull. 26 (2002) 604–608.
[12] S. Ito, K. Nakaoka, M. Kawamura, K. Ui, K. Fujimoto, N. Koura, J. Power Sources 146 (2005) 319–322.
[13] A.R. Armstrong, G. Armstrong, J. Canales, R. Garacia, P.G. Bruce, Adv. Mater. 17 (2005) 862–865.
[14] J.M.D. Coey, A.E. Berkowitz, Li. Balcells, F.F. Putris, F.T. Parker, Appl. Phys. Lett. 72 (1998) 734–736.
[15] M.M. Thackeray, W.I.F. David, J.B. Goodenough, Mater. Res. Bull. 17 (1982) 785–793.
[16] M.M. Thackeray, J. Coetzer, Mater. Res. Bull. 16 (1981) 591–597.
[17] D. Larcher, C. Masquelier, D. Bonnin, Y. Chabre, V. Masson, J.B. Leriche, J.M. Tarascon, J. Electrochem. Soc. 150 (2003) A133–A139.
[18] S. Mitra, P. Poizot, A. Finke, J.M. Tarascon, Adv. Funct. Mater. 16 (2006) 2281–2287.

[19] J.S. Gnanaraj, J.F. DiCarlo, H. Duan, J. Liang, R.W. Thompson, 10th Power Source R&D Symposium, Williamsburg, VA, August 20–23, 2007.
[20] http://www.whatman.com.
[21] P.L. Taberna, S. Mitra, P. Poizot, J.M. Tarascon, Nature Mater. 5 (2006) 567–573.
[22] H.M. Kothari, E.A. Kulp, S.J. Limmer, P. Poizot, E.W. Bohannan, J.A. Switzer, J. Mater. Res. 21 (2006) 293–301.
[23] H. Chik, J. Liang, S.G. Cloutier, N. Koukli, J.M. Xu, Appl. Phys. Lett. 84 (2004) 3376–3378.
[24] J. Liang, H. Chik, J. Xu, IEEE J. Sel. Top. Quantum Electron. 8 (2002) 998–1008.